

## Diverse diterpenoids with $\alpha$ -glucosidase and $\beta$ -glucuronidase inhibitory activities from *Euphorbia milii*

Hang-Fei Yu<sup>a</sup>, Yu-Chen Cheng<sup>b</sup>, Cai-Meng Wu<sup>a</sup>, Kun Ran<sup>a</sup>, Bin Wei<sup>a</sup>, You-Kai Xu<sup>c</sup>, Wei-Guang Shan<sup>a</sup>, You-Min Ying<sup>a,\*\*</sup>, Zha-Jun Zhan<sup>a,\*</sup>

<sup>a</sup> College of Pharmaceutical Science, Zhejiang University of Technology, Hangzhou, 310014, People's Republic of China

<sup>b</sup> Zhejiang University-University of Edinburgh Institute, Haining, 314400, People's Republic of China

<sup>c</sup> Xishuangbanna Tropical Botanical Garden, Chinese Academy of Science, Mengla, 666303, People's Republic of China

### ARTICLE INFO

#### Keywords:

*Euphorbia milii* Des moult.  
Euphorbiaceae  
Rosane  
Diterpenoids  
 $\alpha$ -Glucosidase  
 $\beta$ -Glucuronidase

### ABSTRACT

Four undescribed regular rosane-type diterpenoids euphominoids M–P and three undescribed rearranged rosane-type diterpenoids euphomilonones C–E were isolated from the whole plants of *Euphorbia milii* Des Moul., along with nine known compounds. Their structures were elucidated by detailed interpretation of the NMR and mass spectroscopy. The absolute configurations were established by single-crystal X-ray diffraction experiments, as well as comparative analyses of calculated and experimental ECD spectra. Euphominoid M featured a highly oxygenated ring A and a rare four-membered oxygen ring while euphomilonones C–E possessed 7/5/6 or 5/7/6 fused ring systems, which were rarely occurring in rosane-type diterpenoids. In the *in-vitro* bioassays, 19-norrosal-1,3,5(10),15-tetraene-2,3-diol and antiqurin showed more potent  $\alpha$ -glucosidase inhibitory activity than the positive control acarbose while euphominoid C exhibited significant inhibitory activity against both  $\alpha$ -glucosidase and  $\beta$ -glucuronidase. To the best of our knowledge, it was the first time that rosane-type diterpenoids were reported as  $\beta$ -glucuronidase inhibitors.

### 1. Introduction

The genus *Euphorbia* represents one of the largest genera in the Euphorbiaceae family, consisting more than 2000 species (Shi et al., 2008; Vasaa and Hohmann, 2014). Plants of the genus are traditionally used as herb medicines for the treatment of respiratory disorders, body/skin pain and irritations, indigestion disorders, inflammation, cancer, microbial infestations, snake or scorpion bites, and sensory disorders (Kemboi et al., 2020). Previous phytochemical investigations have revealed that the genus *Euphorbia* is a rich source of diterpenoids (Shi et al., 2008; Vasaa and Hohmann, 2014; Xu et al., 2021). To date, more than 1000 diterpenoids catalogued into 26 normal classes and 37 novel skeleton types have been isolated from the genus (Vasaa and Hohmann, 2014; Xu et al., 2021). In addition to the novel macrocyclic and polycyclic skeletons of *Euphorbia* diterpenoids, incorporation of different oxygen-containing functionalities like aliphatic and aromatic acids also contributes to their structure diversity, which endowed them with a wide range of therapeutically relevant biological activities

including K<sup>+</sup> channel inhibition (Kusz et al., 2016, 2018),  $\alpha$ -glucosidase inhibition (Wei et al., 2018), immunomodulation (Ghanadian et al., 2013; Wan et al., 2016a), anticancer (Yan et al., 2019; Wang et al., 2017), antiviral (Huang et al., 2019; Zhao et al., 2014; Tian et al., 2014; Wang et al., 2018), antimicrobial (Yu et al., 2018; Xu et al., 2015), anti-inflammation (Liang et al., 2019; Zhang et al., 2019; Wan et al., 2016b) antimalarial (Zhou et al., 2016), antifeedant (Hua et al., 2017), multiple drug resistance reversal (Rawal et al., 2014; Hasan et al., 2019; Mai et al., 2018), inhibition of osteoclast formation (Liu et al., 2016), and vasoactive effect (Yang et al., 2013). Among *Euphorbia* diterpenoids, ingenol 3-angelate (ingenol mebutate, PEP005, Picato, LEO Pharma) has attracted the greatest attention since it was approved by the FDA in 2012 and the EMA in 2013 for the treatment of actinic keratosis, a precancerous skin condition (Keating, 2012).

*Euphorbia milii* Des Moul. (Euphorbiaceae) is an ornament plant that has been used as a wart remover. As compared with other plants in the genus, *E. milii* is relatively less studied, with only 12 ingenol esters and 2 phorbol derivatives identified before 2016 (Marston and Hecker, 1983,

\* Corresponding author.

\*\* Corresponding author.

E-mail addresses: [ymying@zjut.edu.cn](mailto:ymying@zjut.edu.cn) (Y.-M. Ying), [zjnpr@zjut.edu.cn](mailto:zjnpr@zjut.edu.cn) (Z.-J. Zhan).

1984; Zani et al., 1993). It was not until recently that Gu et al. (2016) reported the isolation and characterization of 16 undescribed rosane-type diterpenoids from the air parts of *E. milii*, including two rearranged ones featuring a novel 7/5/6 fused-ring system and a novel 5/7/5 tricyclic system, respectively (Liu et al., 2016). The intriguing structures of the rearranged rosane-type diterpenoids prompt us to launch a systematic chemical investigation on the plant. As a result, seven unreported diterpenoids including four regular rosane-type (1–4) and three rearranged rosane-type (5–7), were isolated from the whole plants of *E. milii* along with nine known compounds. This paper describes the isolation, structural elucidation, and characterization of the  $\alpha$ -glucosidase and  $\beta$ -glucuronidase inhibitory activities of diterpenoids 1–16 (Fig. 1).

## 2. Results and discussion

### 2.1. Structural elucidation

A 95% ethanol extract of whole plants of *E. milii* was partitioned between H<sub>2</sub>O and CHCl<sub>3</sub>. The CHCl<sub>3</sub> fraction was subjected to column chromatography over silica gel, MCI gel, and ODS C-18 gel to afford seven previously undescribed rosane-type diterpenoids 1–7, as well as nine known compounds 8–16. The known diterpenoids were identified as 19-norrosa-4,15-diene-6 $\beta$ ,10 $\beta$ -diol-3-one (8) (Gu et al., 2017), 19-norrosa-1,3,5(10),15-tetraene-2,3-diol (9) (Gu et al., 2017), euphominoid B (10) (Liu et al., 2017), euphominoid C (11) (Liu et al., 2017), euphominoid K (12) (Liu et al., 2017), euphominoid A (13) (Liu et al., 2016), euphominoid B (14) (Liu et al., 2016), antiqorin (15) (Min et al., 1989; Cambie et al., 1990), and *ent*-18-hydroxyatis-16-ene-3,14-dione (16) (Lal et al., 1990; Abad et al., 2007; Kuang et al., 2016) by comparing the spectroscopic data with the literature values.

Compound 1 was obtained as colorless crystals with a mp of 188–189 °C. The molecular formula of 1 was determined to be C<sub>20</sub>H<sub>30</sub>O<sub>4</sub> based on the HRESIMS [M + Na]<sup>+</sup> ion at *m/z* 357.2034 (calcd for C<sub>20</sub>H<sub>30</sub>NaO<sub>4</sub>, 357.2036) and the <sup>13</sup>C NMR (Table 1), corresponding to 6 degrees of unsaturation. The IR absorption band at 3462 cm<sup>-1</sup> indicated the existence of three hydroxy groups. The <sup>1</sup>H NMR data (Table 1) showed the resonances for three methyls [ $\delta_{\text{H}}$  0.99 (3H, s), 1.03 (3H, s), 1.15 (3H, s)], one oxymethylene [ $\delta_{\text{H}}$  4.12 (1H, d, *J* = 6.8 Hz), 4.37 (1H, d, *J* = 6.8 Hz)], three oxy-methines [ $\delta_{\text{H}}$  3.53 (1H, d, *J* = 4.7 Hz), 3.58 (1H, dd, *J* = 9.6, 3.8 Hz), 4.35 (1H, m)], one monosubstituted double bond [ $\delta_{\text{H}}$  4.91 (1H, dd, *J* = 17.5, 1.3 Hz), 4.85 (1H, dd, *J* = 10.7, 1.3 Hz), 5.78 (1H, dd, *J* =

17.5, 10.7 Hz)]. The <sup>13</sup>C NMR and DEPT spectra displayed resonances of three methyls ( $\delta_{\text{C}}$  22.7, 19.6, 14.5), seven methylenes ( $\delta_{\text{C}}$  24.6, 26.5, 31.1, 32.0, 39.0, 73.0, 109.2), five methines ( $\delta_{\text{C}}$  36.7, 55.7, 69.7, 70.8, 150.8), and five nonprotonated carbons ( $\delta_{\text{C}}$  36.3, 37.1, 47.5, 65.4, 90.0). The NMR data mentioned above showed characteristics of a rosane-type diterpenoid. In addition, the carbon resonances at  $\delta_{\text{C}}$  55.7 (C-1), 69.7 (C-2), 70.8 (C-3), 90.0 (C-5), and 65.4 (C-10), suggested that 1 is a highly oxygenated molecule.

Preliminary analysis of the <sup>1</sup>H–<sup>1</sup>H COSY, HSQC, and HMBC correlations (Fig. 2) suggested that rings B and C in 1 were closely related to those of euphominoid B (10) (Liu et al., 2017), a rosane-type diterpenoid also obtained in the present study. In the <sup>1</sup>H–<sup>1</sup>H COSY spectrum of 1, correlations of H-1 ( $\delta_{\text{H}}$  3.53)/H-2 ( $\delta_{\text{H}}$  4.35) and H-2 ( $\delta_{\text{H}}$  4.35)/H-3 ( $\delta_{\text{H}}$  3.58) established a main structural fragment –CH(1)–CH(2)–CH(3) in ring A. HMBC correlations between H<sub>3</sub>-20/H-1 and the non-protonated carbon resonance at  $\delta_{\text{C}}$  65.4 defined C-10 as the oxygenated tertiary carbon that was involved in forming an epoxy ring with C-1, while the other oxygenated tertiary carbon was found to be C-5 based on the HMBC correlations between H<sub>2</sub>-6/H<sub>2</sub>-7 and the non-protonated carbon resonance at  $\delta_{\text{C}}$  90.0. The connection between C-3 and C-4 was supported by HMBC correlations between H<sub>3</sub>-18 and C-3/C-4. The oxygenated methylene, anchored at C-4 according to the HMBC correlations between H<sub>2</sub>-19 and C-5/C-4/C-18, was proposed to form an oxetane ring with C-5 via an ether linkage, as implied by the remaining one degree of unsaturation. The planar structure of 1 was thus established. In the NOESY spectrum, NOE correlations (Fig. 3) of H-1/H<sub>b</sub>-11 ( $\delta_{\text{H}}$  0.94), H<sub>b</sub>-11 ( $\delta_{\text{H}}$  0.94)/H<sub>3</sub>-20, H<sub>3</sub>-20/H<sub>2</sub>-19, and H<sub>2</sub>-19/OH-2 suggested that these protons or functional groups possessed the same orientation and were arbitrary assigned as  $\alpha$ -oriented. H-3 was determined to be  $\beta$ -oriented by the NOE correlation of H-3/H<sub>3</sub>-18. Furthermore, NOE correlations of H<sub>a</sub>-11 ( $\delta_{\text{H}}$  1.50)/H<sub>3</sub>-17 and H<sub>3</sub>-17/H-8 indicated H-8 and Me-17 were both in  $\beta$  orientation. The absolute stereochemistry of 1 was determined as 1*R*,2*S*,3*S*,4*R*,5*R*,8*S*,9*S*,10*R*,13*S* by a single-crystal X-ray diffraction experiment with Cu K $\alpha$  radiation (Flack parameter = 0.05(3), CCDC: 2110130) (Fig. 4). Thus, the structure of 1 was proposed as shown in Fig. 1 and named as euphominoid M.

Compound 2 was obtained as white amorphous powder. Its molecular formula was determined as C<sub>20</sub>H<sub>30</sub>O<sub>3</sub> by HRESIMS [M + H]<sup>+</sup> ion at *m/z* 319.2276 (calcd for C<sub>20</sub>H<sub>31</sub>O<sub>3</sub>, 319.2268). The NMR data (Table 1) of 2 resembled those of 5-*epi*-euphominoid J (Liu et al., 2017) except for the replacement of a methylene in 5-*epi*-euphominoid J by an oxygenated methine [ $\delta_{\text{H}}$  4.61 (1H, d, *J* = 2.6 Hz),  $\delta_{\text{C}}$  75.7]. This information, in

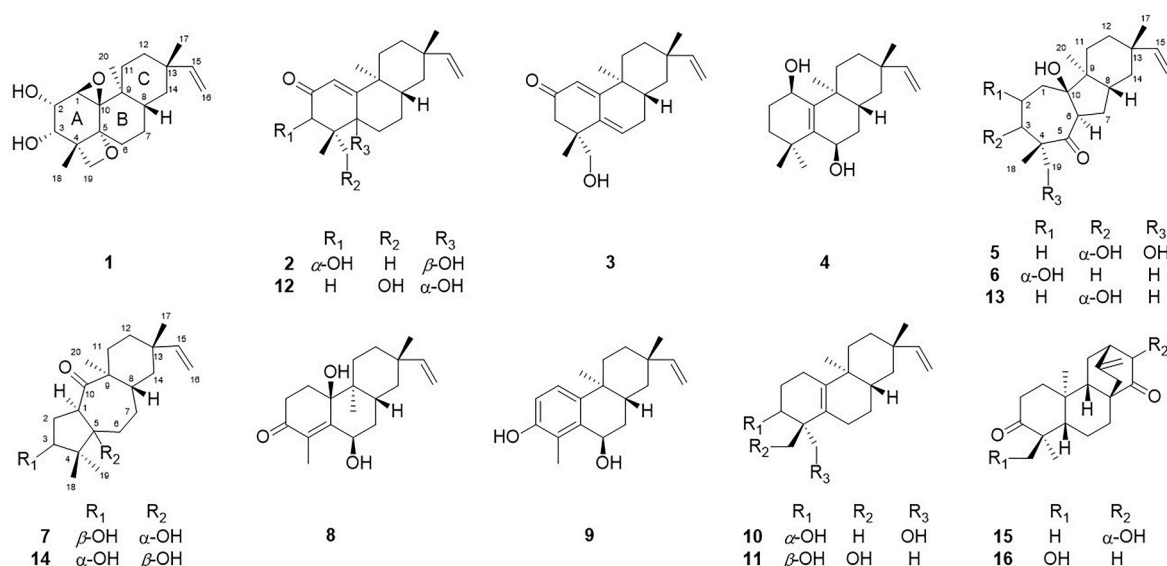


Fig. 1. Chemical structures of 1–16.

**Table 1**  
 $^1\text{H}$  and  $^{13}\text{C}$  NMR spectroscopic data for 1–4.

No.	1		2		3		4	
	$\delta_{\text{C}}^{\text{a}}$	$\delta_{\text{H}}^{\text{b}}$ ( <i>J</i> in Hz)	$\delta_{\text{C}}^{\text{a}}$	$\delta_{\text{H}}^{\text{b}}$ ( <i>J</i> in Hz)	$\delta_{\text{C}}^{\text{a}}$	$\delta_{\text{H}}^{\text{b}}$ ( <i>J</i> in Hz)	$\delta_{\text{C}}^{\text{a}}$	$\delta_{\text{H}}^{\text{b}}$ ( <i>J</i> in Hz)
1	55.7	3.53, d (4.7)	121.1	6.07, s	119.9	5.86, s	63.1	4.16, m
2	69.7	4.35, m	200.7	–	199.7	–	28.7	1.78, m 1.74, m
3	70.8	3.58, dd (9.6, 3.8)	75.7	4.61, d (2.6)	47.1	2.44, d (16.5) 2.40, d (16.5)	33.3	1.91, td (14.0, 3.4) 1.35, m
4	47.5	–	48.2	–	43.2	–	34.9	–
5	90.0	–	76.8	–	135.7	–	139.7	–
6	32.0	2.42, ddd (14.2, 3.1, 3.1) 1.74, ddd (13.1, 13.1, 4.8)	24.2	1.90, dd (7.3, 2.2) 1.89, d (5.1)	131.6	6.08, m	64.4	4.18, m
7	24.6	1.64, m 1.37, m	22.6	1.74, m 1.28, m	31.2	2.19, dt (18.9, 5.1) 1.95, ddd (19.0, 11.2, 2.0)	35.3	1.47, m 1.55, m
8	36.7	1.64, m	29.4	2.30, m	35.0	1.88, m	31.6	2.15, m
9	37.1	–	38.6	–	37.4	–	39.0	–
10	65.4	–	172.1	–	164.6	–	143.2	–
11	26.5	1.50, m 0.94, m	34.2	1.80, m 1.58, m	31.4	1.67, m 1.63, m	31.7	1.68, m 1.58, m
12	31.1	1.52, m 1.23, m	32.6	1.59, m 1.38, m	32.5	1.59, dd (12.7, 4.5) 1.42, dt (9.8, 2.6)	32.8	1.67, m 1.35, m
13	36.3	–	36.3	–	36.2	–	36.5	–
14	39.0	1.34, m 1.11, dt (13.3, 2.7)	39.9	1.25, m 1.24, m	39.2	1.37, d (12.8) 1.21, m	39.4	1.44, m 1.10, m
15	150.8	5.78, dd (17.5, 10.7)	150.6	5.82, dd (17.5, 10.7)	150.5	5.81, dd (17.5, 10.8)	151.1	5.82, dd (17.5, 10.7)
16	109.2	4.91, dd (17.5, 1.3) 4.85, dd (10.7, 1.3)	109.4	4.95, dd (17.5, 1.3) 4.89, dd (10.7, 1.3)	109.5	4.95, dd (17.5, 1.1) 4.89, dd (10.8, 1.1)	109.0	4.94, dd (17.5, 1.3) 4.86, dd (10.7, 1.3)
17	22.7	0.99, s	22.5	1.02, s	22.3	1.00, s	23.5	1.08, s
18	19.6	1.15, s	18.8	1.22, s	23.1	1.23, s	29.6	1.22, s
19	73.0	4.37, d (6.8) 4.12, d (6.8)	17.2	0.78, s	68.6	3.40, d (10.8) 3.36, d (10.8)	27.7	0.98, s
20	14.5	1.03, s	19.2	1.01, s	16.8	0.92, s	17.2	0.83, s
OH-2	–	3.12, d (11.6)	–	–	–	–	–	–
OH-3	–	2.54, d (9.6)	–	3.46, d (2.6)	–	–	–	–
OH-5	–	–	–	1.67, s	–	–	–	–

<sup>a</sup> Measured at 150 MHz in  $\text{CDCl}_3$ .

<sup>b</sup> Measured at 600 MHz in  $\text{CDCl}_3$ ; Proton coupling constant (*J*) in Hz are given in parentheses. The assignments were based on  $^1\text{H}$ - $^1\text{H}$  COSY, HSQC, and HMBC experiments.

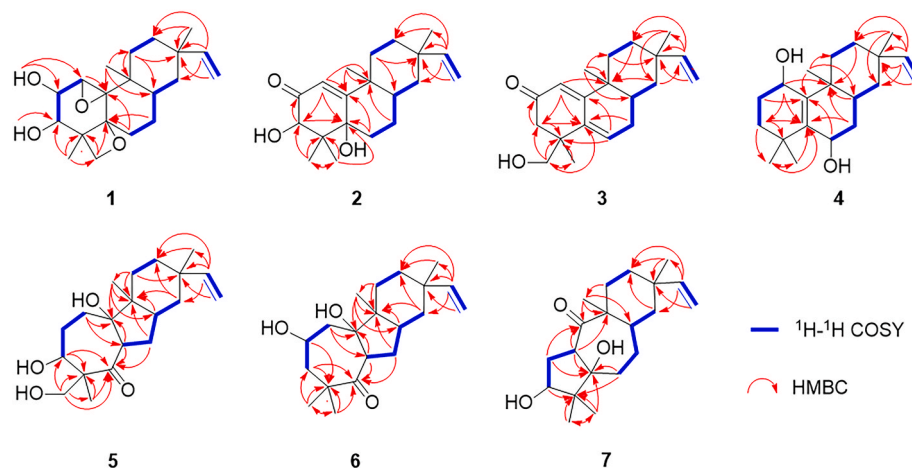


**Fig. 2.** Key  $^1\text{H}$ - $^1\text{H}$  COSY (blue bold bonds) and HMBC (red arrows) correlations of 1–7. (For interpretation of the references to color in this figure legend, the reader is referred to the Web version of this article.)

combination with the molecular formula, suggested the existence of another hydroxy in 2 as compared with 5-*epi*-euphominoid J. By comprehensive elucidation of the 2D NMR (Fig. 2) spectra, a rosane skeleton with an  $\alpha,\beta$ -unsaturated ketone moiety in ring A and a hydroxy substituted C-5 could be easily established. The proton of the additional hydroxy in 2 appeared as a double doublet [ $\delta_{\text{H}}$  3.46 (1H, d, *J* = 2.6 Hz)] in the  $^1\text{H}$  NMR spectrum, which was found to correlate with the oxygenated methine proton H-3 ( $\delta_{\text{H}}$  4.61) in the  $^1\text{H}$ - $^1\text{H}$  COSY spectrum, suggesting the location of the hydroxy at C-3. The postulation was

further confirmed by HMBC correlations between OH-3 and C-2/C-3, and between H-1/H<sub>3</sub>-18 and C-3. The NOESY spectrum (Fig. 3) of 2 displayed correlations of H-8/OH-5 and OH-5/H-3, suggesting a  $\beta$ -orientation for OH-5 and an  $\alpha$ -orientation for OH-3. The absolute configuration of 2 was established by comparison of the experimental and calculated electronic circular dichroism (ECD) spectra. The calculated ECD curve for 3*S*,5*R*,8*S*,9*S*,13*S*-enantiomer was in good agreement with the experimental ECD spectrum (Fig. 5). Thus, the structure of 2 was established as shown in Fig. 1 and named as euphominoid N.

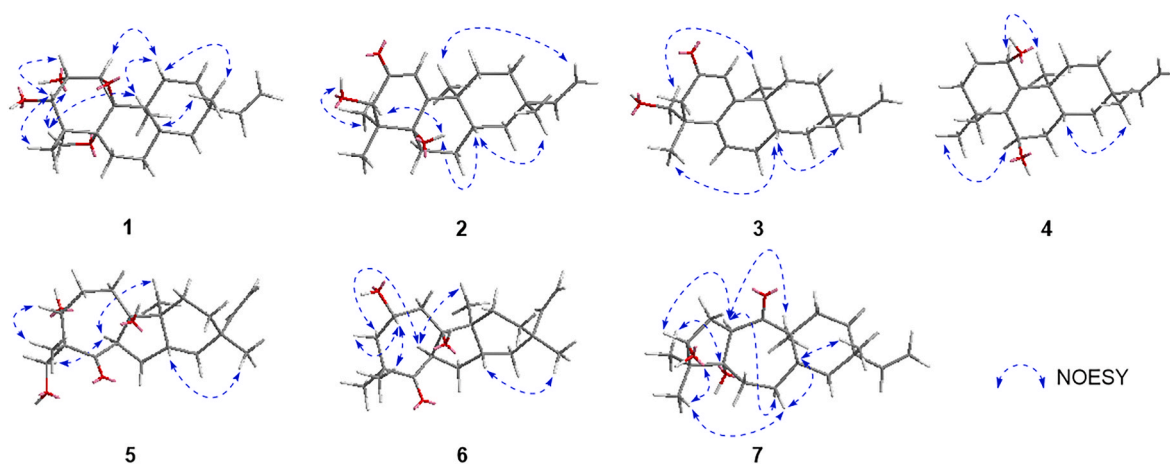


Fig. 3. Key NOE correlations (blue dashed arrows) in 1–7. (For interpretation of the references to color in this figure legend, the reader is referred to the Web version of this article.)

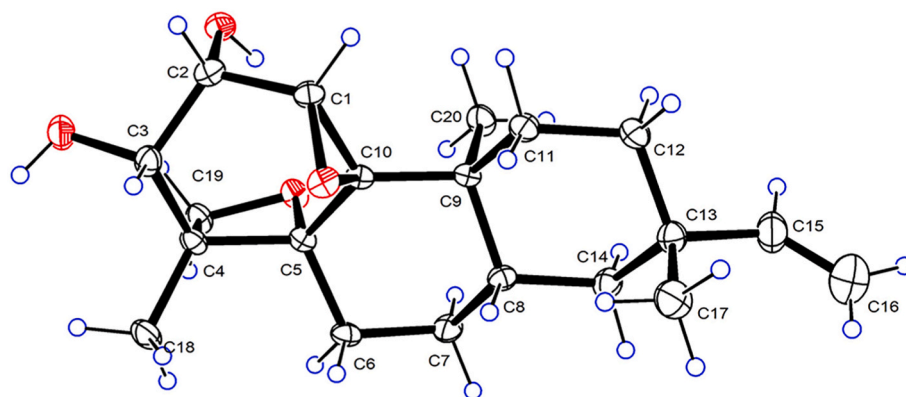


Fig. 4. ORTEP diagram of 1.

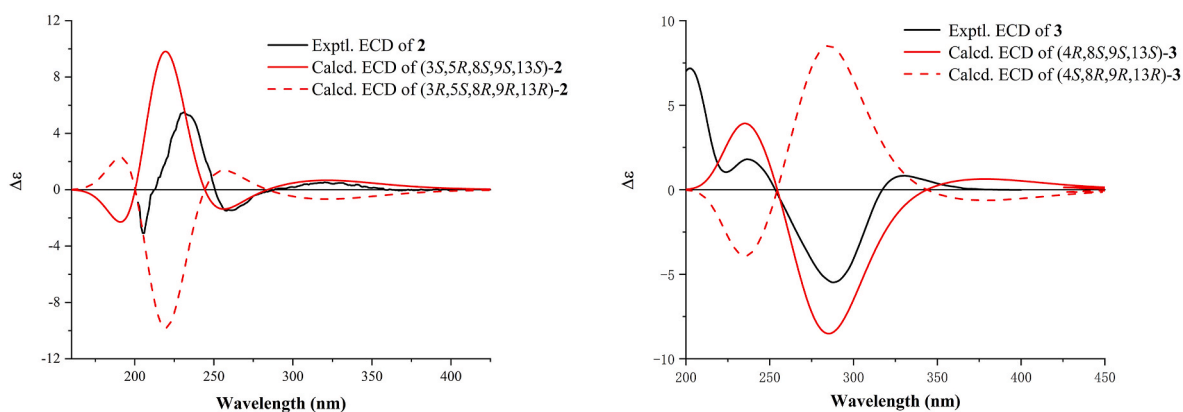


Fig. 5. Experimental and calculated ECD curves of 2 and 3.

Compound 3, pale-yellow oil, had the molecular formula  $C_{20}H_{28}O_2$  as determined by HRESIMS [ $M + H$ ] $^+$  ion at  $m/z$  301.2176 (calcd for  $C_{20}H_{29}O_2$ , 301.2162). Comparison of the  $^1H$  and  $^{13}C$  NMR data of 3 (Table 1) with those of the known rosane-type diterpenoid 18-hydroxy-3-deoxyhugosone (Baraza et al., 2008) revealed the structure similarity between them, except for the disappearance of signals for one methylene and one methine in 18-hydroxy-3-deoxyhugosone and the presence of a tri-substituted double bond [ $\delta_H$  6.08 (1H, m),  $\delta_C$  131.6 and 135.7] that was proposed to be located between C-5 and C-6 based

on the  $^1H$ - $^1H$  COSY correlation of H-6 ( $\delta_H$  6.08)/H<sub>2</sub>-7 and confirmed by HMBC correlations between H-6 ( $\delta_H$  6.08) and C-4/C-10, and between H-1/H<sub>2</sub>-3 and C-5. In the NOESY spectrum, NOE correlations (Fig. 3) of H-8 ( $\delta_H$  1.88)/H<sub>3</sub>-17 ( $\delta_H$  1.00) and H<sub>3</sub>-20 ( $\delta_H$  0.92)/H<sub>2</sub>-19 were observed, indicating that CH<sub>2</sub>-19 and Me-20 were  $\alpha$ -oriented while H-8 and Me-17 were  $\beta$ -oriented. The absolute configuration of 3 was determined to be 4R,8S,9S,13S by comparison of the experimental and calculated ECD spectra (Fig. 5). Thus, 3 was determined to possess the structure as shown in Fig. 1 and named as euphominoid O.

Compound **4** was isolated as colorless crystals with a mp of 231–232 °C. A molecular formula of  $C_{20}H_{32}O_2$  was ascertained for **4** from the HRESIMS  $[M + Na]^+$  ion at  $m/z$  327.2300 (calcd for  $C_{20}H_{32}NaO_2$ , 327.2295). The  $^1H$  and  $^{13}C$  NMR data (Table 1) of **4** were closely related to those of euphominoid H (Liu et al., 2017). The obvious differences were the presence of one additional oxygenated methine [ $\delta_H$  4.16 (1H, m),  $\delta_C$  63.1] in **4**, replacing the carbonyl ( $\delta_C$  198.1) in euphominoid H. Therefore, **4** was proposed to be originated from euphominoid H via ketone reduction at C-1, which was verified by  $^1H$ - $^1H$  COSY correlation of H-1 ( $\delta_H$  4.16)/H<sub>2</sub>-2 and HMBC correlations between H-1 ( $\delta_H$  4.16) and C-3/C-5/C-9. Due to the overlap of proton resonances for H-1 and H-6, the relative configurations at C-1 and C-6 of **4** could not be determined by NOESY experiment. Fortunately, we obtained the single crystal of **4** and subjected it to X-ray diffraction, results of which confirmed the planar structure and determined the absolute configuration of **4** as 1*R*,6*R*,8*R*,9*S*,13*S* (Flack parameter = 0.12(5), CCDC: 2110133, Fig. 6). Compound **4** was named as euphominoid P.

Compound **5**, colorless crystals with a mp of 185–186 °C, was determined to possess a molecular formula of  $C_{20}H_{32}O_4$  by HRESIMS  $[M + Na]^+$  ion at  $m/z$  359.2207 (calcd for  $C_{20}H_{32}NaO_4$ , 359.2193). The  $^1H$  and  $^{13}C$  NMR data of **5** (Table 2) showed partial characteristics of a rosane-type diterpenoid with slight deviations. Comparative elucidation of the NMR data indicated that **5** was closely related to euphominone A (**13**) (Liu et al., 2016) a rearranged rosane-type diterpenoid possessing a 7/5/6 tricyclic system. The key difference was the replacement of a methyl singlet in euphominone A (**13**) by an oxygenated methylene in **5**. In the HMBC spectrum, proton resonances of the oxygenated methylene [ $\delta_H$  3.98 (1H, m), 3.67 (1H, d,  $J = 10.4$  Hz)] showed correlations with C-3, C-4, and C-5, anchoring the oxygenated methylene at C-4. The relative configuration of **5** was deduced from the NOESY spectrum. The NOE correlations (Fig. 3) of H<sub>3</sub>-20/H-6 and H-6/H<sub>2</sub>-19 suggested these protons or functional groups were  $\alpha$ -oriented, while H-3 and H<sub>3</sub>-18 were deduced as  $\beta$ -oriented based on the NOE correlation of H-3/H<sub>3</sub>-18. Since no proton signal for OH-10 was present in the  $^1H$  NMR spectrum, the orientation of OH-10 could not be determined by NOESY experiment. Fortunately, a single crystal of **5** was obtained from  $CHCl_3/MeOH/n$ -hexane/EtOAc (1:1:2:1). Hence, the absolute stereochemistry of **5** was identified as 3*R*,4*R*,6*R*,8*S*,9*S*,10*R*,13*S* (Fig. 7) through a single crystal X-ray experiment with Cu K $\alpha$  radiation (Flack parameter: 0.00(17), CCDC: 2,110,134). Compound **5** was named as euphominone C.

Compound **6** was also isolated as colorless crystals with a mp of 224–225 °C. Its molecular formula was determined as  $C_{20}H_{32}O_3$  by HRESIMS  $[M + Na]^+$  ion at  $m/z$  343.2236 (calcd for  $C_{20}H_{32}NaO_3$ ,

343.2244). Preliminary analysis of the  $^1H$  and  $^{13}C$  NMR data (Table 2) indicated that **6** was closely related to euphominone A (**13**) (Liu et al., 2016). After detailed elucidation of the 2D NMR spectra, a rearranged rosane skeleton with the same 7/5/6 fused-ring system as that in euphominone A (**13**) was established for **6**. However, the oxygenated methine was deduced to be anchored at C-2 based on the  $^1H$ - $^1H$  COSY correlations of H<sub>2</sub>-1/H-2 ( $\delta_H$  4.11) and H-2 ( $\delta_H$  4.11)/H<sub>2</sub>-3, as well as the HMBC correlations between H<sub>2</sub>-1 and C-6/C-10, H-2 and C-4, H<sub>2</sub>-3 and C-4/C-5, and H<sub>3</sub>-18/H<sub>3</sub>-19 and C-3. In the NOESY spectrum, NOE correlations (Fig. 3) of H<sub>3</sub>-20/H-6 and H-6/H<sub>a</sub>-3 ( $\delta_H$  2.07) indicated these protons or functional groups were in  $\alpha$ -orientation. Consequently, the additional NOE correlation of H<sub>b</sub>-3 ( $\delta_H$  1.79)/H-2 defined a  $\beta$ -orientation of H-2. The orientation of OH-10 could not be determined by NOESY experiment as in the case of **5**. The absolute stereochemistry of **6** was determined to be 2*S*,6*R*,8*S*,9*S*,10*R*,13*S* (Fig. 8) by a single crystal X-ray experiment with Cu K $\alpha$  radiation (Flack parameter: 0.05(2), CCDC: 2, 110,135) since we obtained the single crystal of **6** in  $CHCl_3$ . Compound **6** was named as euphominone D.

Compound **7**, white amorphous powder, had the same molecular formula ( $C_{20}H_{32}O_3$ ) with euphominones B (**14**) (Liu et al., 2016) and D (**6**) as deduced by HRESIMS  $[M + H]^+$  ion at  $m/z$  321.2432 (calcd for  $C_{20}H_{33}O_3$ , 321.2424). Compound **7** was proposed to share the same 5/7/6 fused tricyclic rosane skeleton with that of euphominone B (**14**) by comparative analysis of the  $^1H$  and  $^{13}C$  NMR data (Table 2). Further in-depth elucidation of the  $^1H$ - $^1H$  COSY, HSQC, and HMBC spectra of **7** (Fig. 2) allowed the establishment of its planar structure that was found to be identical with that of euphominone B (**14**), suggesting they were stereoisomers. The relative stereochemistry of **7** was determined based on biogenetic consideration and NOESY experiment. The 5/7/6 tricyclic skeleton in euphominone B (**14**) was proposed to be derived from the normal 6/6/6 fused rosane skeleton via biosynthetic pathways without alteration to the ring C. Therefore, H<sub>3</sub>-20 was  $\alpha$ -oriented, while H-8 and H<sub>3</sub>-17 were in  $\beta$  orientation. In the NOESY spectrum of **7**, NOE correlations (Fig. 3) of H-8/H<sub>b</sub>-7, H<sub>b</sub>-7/H<sub>3</sub>-18 and H<sub>3</sub>-18/OH-3 were observed, suggesting the  $\beta$  orientation of these protons or functional groups. Additional NOE correlations of H-3/H<sub>3</sub>-19, H<sub>3</sub>-19/OH-5, and H<sub>a</sub>-7/H-1 demonstrated they were  $\alpha$  oriented. The absolute configuration of **7** was determined to 1*R*,3*S*,5*S*,8*S*,9*S*,13*S* by ECD calculation at the B3LYP/6-31G(d) level using the Gaussian 09 program (Fig. 9).

## 2.2. Bioassay

The  $\alpha$ -glucosidase inhibitory activity of all the compounds was

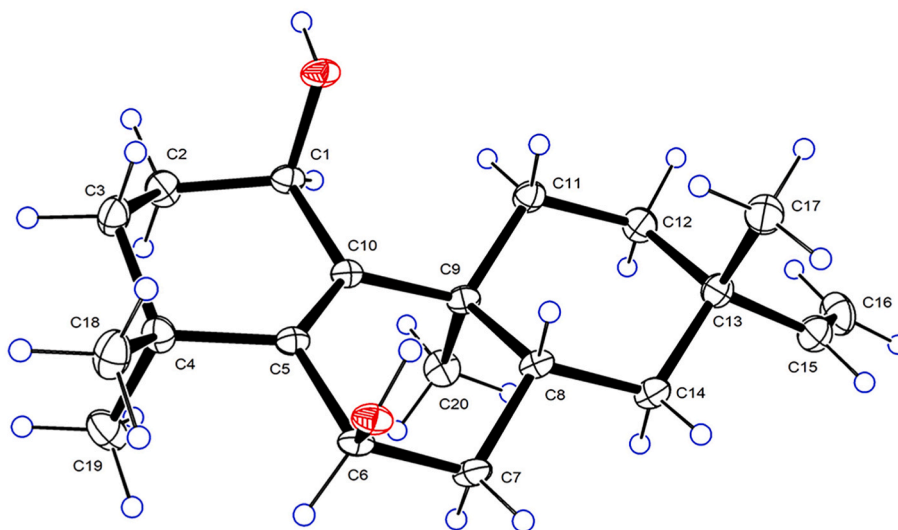


Fig. 6. ORTEP diagram of **4**.

**Table 2**  
<sup>1</sup>H and <sup>13</sup>C NMR spectroscopic data for 5–7.

No.	5		6		7	
	$\delta_c^a$	$\delta_H^b$ (J in Hz)	$\delta_c^a$	$\delta_H^b$ (J in Hz)	$\delta_c^c$	$\delta_H^d$ (J in Hz)
1	27.9	2.32, td (13.6, 4.1) 1.54, m	43.9	2.13, ddd (15.7, 12.9, 1.4) 1.70, dd (12.9, 10.6)	55.3	3.48, t (8.7)
2	26.0	2.15, m 1.94, m	66.1	4.11, m	30.7	2.28, ddd (12.6, 11.3, 8.7) 1.71, m 4.14, m
3	76.8	4.10, d (6.5)	49.1	2.07, dd (14.5, 11.2) 1.79, dt (14.5, 1.8)	77.5	4.14, m
4	54.5	–	45.6	–	50.0	–
5	213.8	–	214.9	–	83.3	–
6	59.4	3.96, m	54.3	3.61, dd (10.3, 3.3)	27.9	1.73, m 1.24, m
7	26.3	2.41, ddd (12.9, 7.9, 3.4) 1.14, m	27.1	2.24, ddd (12.8, 7.9, 3.3) 1.14, m	32.6	2.76, m 1.58, m
8	38.1	2.06, m	38.0	2.01, m	33.1	1.11, m
9	49.2	–	49.2	–	50.0	–
10	84.6	–	84.1	–	215.2	–
11	29.9	1.25, m 1.21, m	26.4	1.62, td (13.2, 4.1) 1.19, m	29.4	1.56, m 1.20, m
12	32.2	1.56, m 1.27, m	32.1	1.52, m 1.30, m	32.3	1.27, m (2H)
13	37.1	–	37.2	–	37.1	–
14	36.4	1.37, m (2H)	36.3	1.37, m (2H)	40.3	1.29, m 1.21, m
15	151.0	5.82, dd (17.5, 10.7)	150.8	5.82, dd (17.5, 10.7)	151.5	5.84, dd (17.5, 10.8)
16	109.1	4.94, dd (17.5, 1.2) 4.86, dd (10.7, 1.2)	109.2	4.93, dd (17.5, 1.3) 4.86, dd (10.7, 1.3)	109.6	4.95, dd (17.5, 1.2) 4.85, dd (10.8, 1.2)
17	23.6	1.01, s	23.5	1.00, s	22.9	1.07, s
18	19.7	1.04, s	29.8	1.05, s	15.7	0.57, s
19	73.9	3.98, m 3.67, d (10.4)	23.6	1.23, s	20.3	0.90, s
20	14.5	0.79, s	14.6	0.77, s	13.5	1.01, s
OH- 3	–	–	–	–	–	3.65, d (6.0)
OH- 5	–	–	–	–	–	3.57, s

<sup>a</sup> Measured at 150 MHz in CDCl<sub>3</sub>.

<sup>b</sup> Measured at 600 MHz in CDCl<sub>3</sub>.

<sup>c</sup> Measured at 150 MHz in acetone-d<sub>6</sub>.

<sup>d</sup> Measured at 600 MHz in acetone-d<sub>6</sub>; Proton coupling constant (*J*) in Hz are given in parentheses. The assignments were based on <sup>1</sup>H–<sup>1</sup>H COSY, HSQC, and HMBC experiments.

evaluated employing acarbose as a positive control. Compounds **9**, **11** and **15** inhibited the activity of  $\alpha$ -glucosidase with IC<sub>50</sub> values of 48.48 ± 2.06, 52.50 ± 2.31, 89.32 ± 1.87  $\mu$ M, respectively, compared to an IC<sub>50</sub> value of 422.3 ± 8.44  $\mu$ M for acarbose (Table 3 and Fig. 11). Furthermore, the inhibition kinetics of **9**, **11** and **15** were studied, as shown in Fig. 11. Based on the observed inhibition kinetics and the x-intercept of the Lineweaver–Burk plots of **9** and the y-intercept of the Lineweaver–Burk plots of **11** and **15**, it was concluded that **9** acted via a noncompetitive inhibition mechanism while **11** and **15** acted via a competitive inhibition mode.

*E. coli*  $\beta$ -glucuronidase (EcGUS) is one of the most abundant and most efficient bacterial  $\beta$ -glucuronidases that have been reported to cause severe gut toxicities that limit the efficacy of cancer drugs and other therapeutics (Wallace et al., 2010, 2015; Bhatt et al., 2020). Inhibitors of

EcGUS may alleviate these side effects. In the present study, the inhibitory effects of **1–16** against EcGUS were investigated using D-saccharic acid 1,4-lactone (DSL) as the positive control. As a result, **11** inhibited EcGUS with an IC<sub>50</sub> value of 45.87 ± 1.94  $\mu$ M, comparable to the positive control DSL (IC<sub>50</sub> = 50.64 ± 5.03  $\mu$ M) (Table 3 and Fig. 10). In Lineweaver–Burk plots, the location of the intercept of regression lines in the second quadrant demonstrated that **11** was a mixed-type inhibitor of EcGUS (Fig. 11).

The rosane-type diterpenoids belong to the higher diterpenoids of the genus *Euphorbia*, which usually possess 6/6/6 fused ring systems. The chemical diversity of these diterpenoids is mainly derived from different patterns of substitutions in ring A by oxygen-containing functional groups (Vasaa et al., 2014; Kemboi et al., 2014). Euphominoid **M** (**1**) was obtained as a highly oxygenated compound incorporating vicinal diols, oxetane, and epoxy moieties in ring A simultaneously. It was quite rare that these oxygen-containing functionalities co-exist in ring A of a rosane-type diterpenoid. In addition, to the best of our knowledge, euphominoid **M** (**1**) was the first rosane-type diterpenoid that possessed an ether linkage between C-19 and C-5. Euphomilones C–E (**5–7**) were elucidated to have unusual 7/5/6 or 5/7/6 fused tricyclic rosane-skeletons that were proposed to be originated from the regular rosane skeleton via oxidation followed by nucleophilic addition (Liu et al., 2016). To date, all the five diterpenoids with these two types of rearranged rosane skeletons have been characterized from *E. milii*, including euphomilones A–B (**13–14**) (Liu et al., 2016). The isolation and identification of euphomilones C–E (**5–7**) in the present study further enriched their structure diversity. As compared with the wide distribution of other diterpenoids in the genus *Euphorbia*, the solitary occurrence of the 7/5/6 and 5/7/6 fused tricyclic rosane-skeletons in *E. milii* suggested the potential significance of these diterpenoids in the chemotaxonomy of this plant. In the in-vitro bioassays, compounds **9**, **11**, and **15** showed more active inhibitory activity against  $\alpha$ -glucosidase than positive control acarbose. Additionally, compound **11** exhibited significant inhibitory activity against EcGUS, a potential target for drug-related gastrointestinal toxicity (Wallace et al., 2010, 2015; Bhatt et al., 2020). It was worth noting that **11** represent the first discovered rosane-type diterpenoid with good EcGUS inhibitory activity.

### 3. Conclusion

In the present study, four undescribed regular (**1–4**) and three undescribed rearranged rosane-type diterpenoids (**5–7**) were isolated from the whole plant of *E. milii* along with nine known compounds. Compound **1** featured a highly oxygenated ring A and a rare four-membered oxygen ring while compounds **5–7** possessed 7/5/6 or 5/7/6 fused ring systems, which were rarely occurring in rosane-type diterpenoids. In the in-vitro bioassays, compounds **9** and **15** showed more potent  $\alpha$ -glucosidase inhibitory activity than the positive control acarbose while **11** exhibited significant inhibitory activity against both  $\alpha$ -glucosidase and  $\beta$ -glucuronidase. To the best of our knowledge, it was the first time that rosane-type diterpenoids were reported as  $\beta$ -glucuronidase inhibitors.

### 4. Experimental

#### 4.1. General experimental procedures

Melting points were obtained on a Beijing Tech X-5 microscopic melting point apparatus (uncorrected). Optical rotations were obtained with a Rudolph Research Autopol III automatic polarimeter. UV spectra were measured on a TU-1900 spectrometer (Persee, Beijing, China). IR spectra were recorded on a Thermo Nicolet 6700 FT-IR microscope instrument (FT-IR microscope transmission) in KBr pellets. ECD measurements were determined on a JASCO J-815 spectropolarimeter (JASCO, Kyoto, Japan). 1D and 2D-NMR spectra were obtained at 600 MHz for <sup>1</sup>H and 150 MHz for <sup>13</sup>C on a Bruker Avance 600 spectrometer,

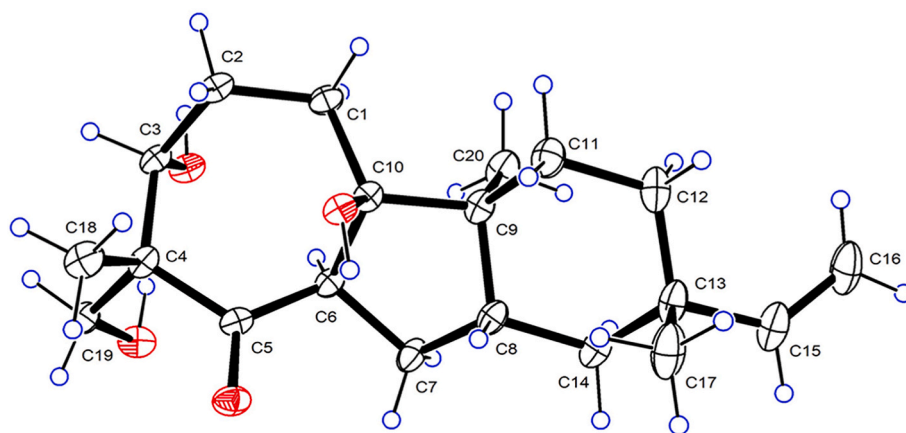


Fig. 7. ORTEP diagram of 5.

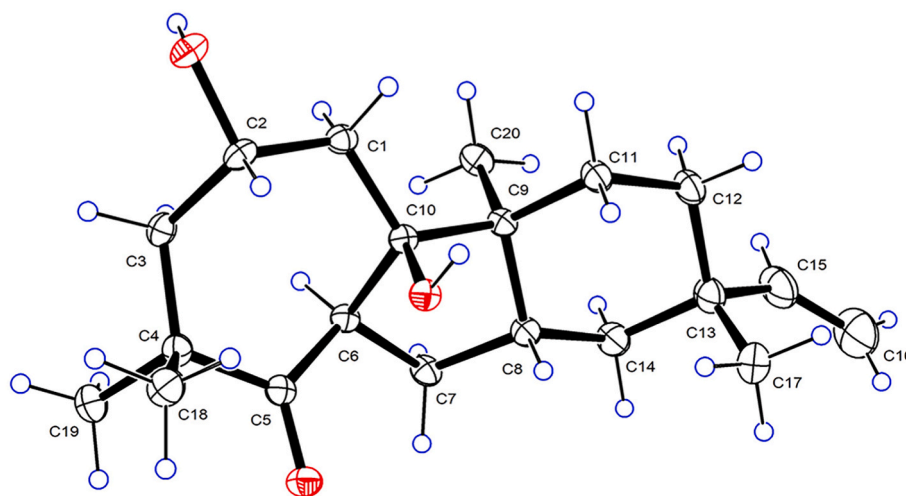


Fig. 8. ORTEP diagram of 6.

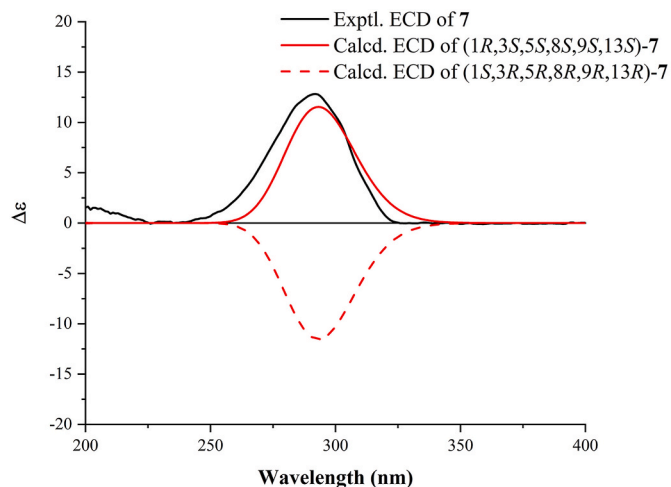


Fig. 9. Experimental and calculated ECD curves of 7.

in methanol- $d_4$ ,  $CDCl_3$  or acetone- $d_6$ , with solvent peaks used as references. ESIMS and HRESIMS data were measured on an Agilent-6210-LC/TOF mass spectrometer (Agilent Technologies, Inc., California, USA). The X-ray crystallographic data were collected on an Agilent Xcalibur Atlas Gemini Ultra diffractometer using  $Cu\ K\alpha$  radiation. Column

**Table 3**  
 $\alpha$ -Glucosidase and  $\beta$ -glucuronidase Inhibitory Activities of 9, 11, and 15.

compounds	$IC_{50}^a$ ( $\mu M$ )	
	$\alpha$ -glucosidase	$\beta$ -glucuronidase
9	$48.48 \pm 2.06$	–
11	$52.50 \pm 2.31$	$45.87 \pm 1.94$
15	$89.32 \pm 1.87$	–
acarbose <sup>b</sup>	$422.3 \pm 8.44$	–
DSL <sup>c</sup>	–	$50.64 \pm 5.03$

<sup>a</sup> All sixteen diterpenoids were evaluated in the preliminary screening at a concentration of 100  $\mu M$  and those with inhibition rates lower than 50% were regarded as non-active and discarded before further screening. Results are presented as means  $\pm$  SD at three independent experiments.

<sup>b</sup> Acarbose was used as the positive control in the  $\alpha$ -glucosidase inhibitory assay.

<sup>c</sup> D-Saccharic acid 1,4-lactone (DSL) was used as the positive control in the  $\beta$ -glucuronidase inhibitory assay.

chromatography (CC) was performed on silica gel ( $SiO_2$ ; 200–300 mesh; Qingdao Marine Chemical Co., Ltd.), ODS C-18 gel (50 mm; YMC Co., Ltd., Kyoto, Japan), MCI CHP 20 P gel (75–150  $\mu m$ , Tokyo, Japan). Thin layer chromatography (TLC) was performed on precoated silica gel GF254 plates (Qingdao Marine Chemical Co., Ltd., Qingdao, China) and visualized by UV light and/or spraying with 10%  $H_2SO_4$  in 95% EtOH followed by heating. Both  $\alpha$ -glucosidase and  $\beta$ -glucuronidase inhibitory

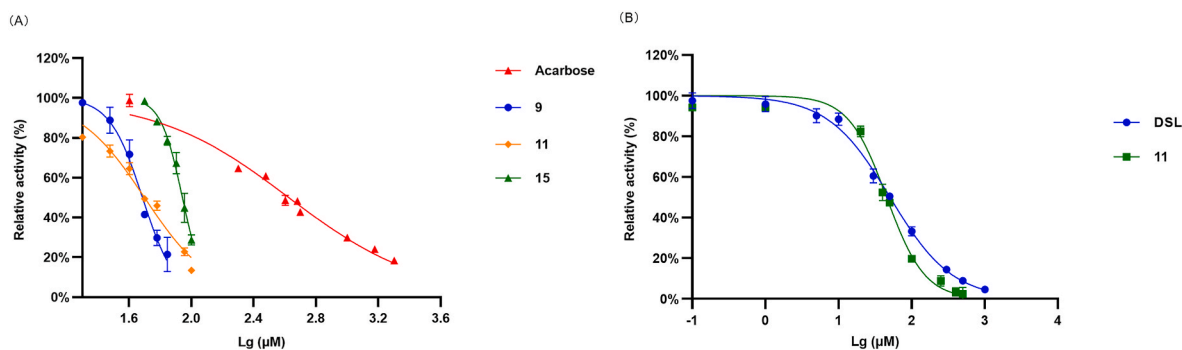


Fig. 10. The dose-dependent inhibition curves of inhibitors on PNPG-hydrolyzing activity of  $\alpha$ -glucosidase (A) and EcGUS (B). All data were expressed as mean  $\pm$  SD of triplicate reactions.

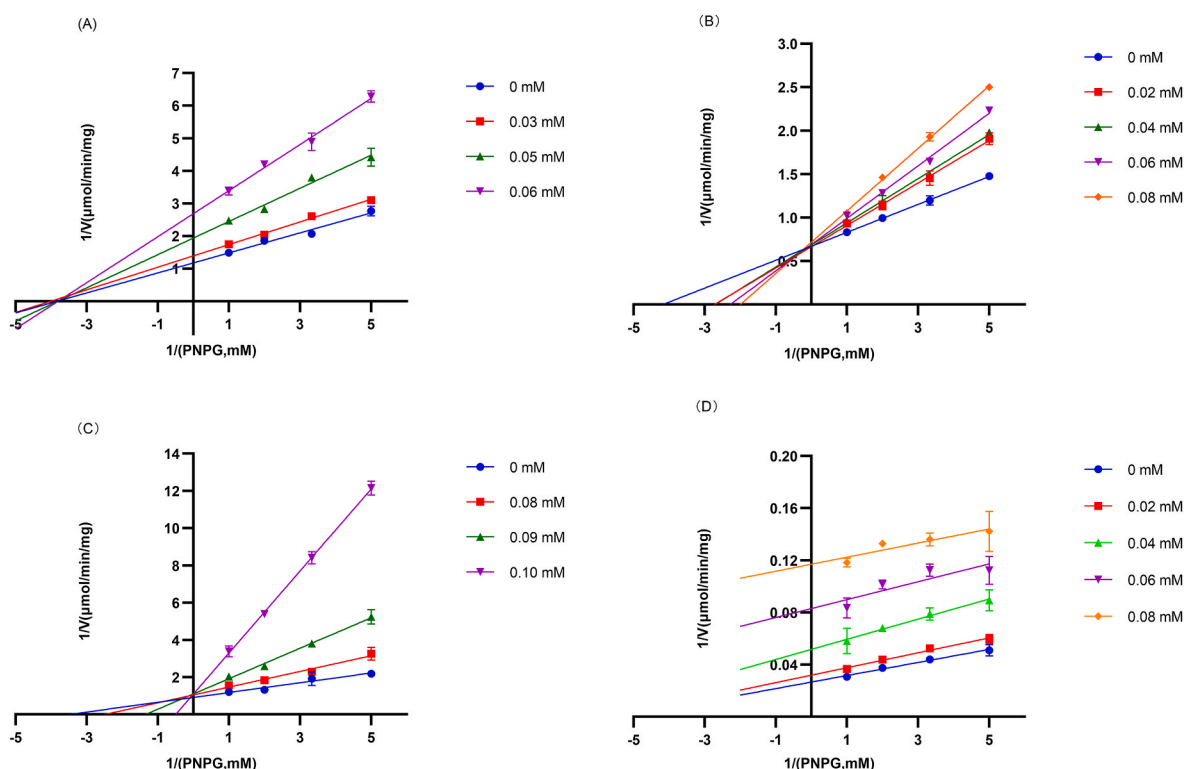


Fig. 11. The Lineweaver-Burk plots of (A) 9, (B) 11, and (C) 15 against acarbose and 11 against DSL (D). All data were expressed as mean  $\pm$  SD of triplicate reactions.

activities were measured spectrophotometrically using a SpectraMax Plus 384 microplate reader (Molecular Devices, CA, USA). All reagents used for biological evaluation were provided by Sigma-Aldrich. All solvents used were of analytical grade and obtained from commercially available sources.

#### 4.2. Plant material

The whole plants of *Euphorbia milii* Des Moul. (Euphorbiaceae) were collected in Xishuangbanna tropical botanical garden, Chinese Academy of Sciences, Mengla, Yunnan Province, People's Republic of China, in June of 2017 and authenticated by Dr. Youkai Xu at Xishuangbanna tropical botanical garden, Chinese Academy of Sciences. A voucher specimen (No. ZJUT EM20170601) has been deposited at the Institute of Natural Medicine, College of Pharmaceutical Science, Zhejiang University of Technology.

#### 4.3. Extraction and isolation

The whole plants of *E. milii* (3.0 Kg) were dried and percolated with 95% ethanol at room temperature three times ( $3 \times 20$  L, 7 d each) to afford a crude extract (365 g) after removal of the solvent under reduced pressure at 35 °C. The crude extract was partitioned between water and  $\text{CHCl}_3$ . The concentrated  $\text{CHCl}_3$  layer (222 g) was subjected to silica gel column chromatography (CC) eluting with a gradient of petroleum ether/EtOAc (20:1, 15:1, 10:1, 7:1, 5:1, 4:1, 3:1, 2:1, 1:1, v/v) to give nine fractions (Fr. A–I). Fr. I (23.5 g) was chromatographed over MCI CHP20P gel eluting with a gradient of MeOH/H<sub>2</sub>O (60:40  $\rightarrow$  90:10, v/v) to yield ten fractions (I1–I10). Fr. I2 was further separated on an ODS C-18 column eluting with a gradient of MeOH/H<sub>2</sub>O (30:20  $\rightarrow$  40:10, v/v) to furnish sixteen fractions (Fr. I2A–I2P). Fr. I2F was purified by silica gel CC eluting with  $\text{CHCl}_3$ /EtOAc (50:1, v/v) to give 15 (16.0 mg). 16 (14.8 mg) was obtained from Fr. I2G by recrystallization in  $\text{CHCl}_3$ . Fr. I2M was chromatographed over silica gel eluting with a gradient of  $\text{CHCl}_3$ /MeOH (60:1  $\rightarrow$  40:1, v/v) to offer 6 (18.6 mg) and 7 (22.3 mg).

14 (5.8 mg) was obtained from Fr. I2P by CC over silica gel eluting with a gradient of  $\text{CHCl}_3/\text{MeOH}$  (60:1  $\rightarrow$  40:1, v/v). Fr. I5 was loaded onto an ODS C-18 column eluting with a gradient of  $\text{MeOH}/\text{H}_2\text{O}$  (65:35  $\rightarrow$  90:10, v/v) to give fourteen fractions (Fr. I5A–I5N). Fr. I5G, I5M, and I5N were purified by silica gel CC eluting with  $\text{CHCl}_3/\text{MeOH}$  (50:1, v/v) to furnish **12** (28.6 mg), **10** (3.7 mg), and **11** (46.3 mg), respectively. Fr. I5H was chromatographed over ODS C-18 eluting with a gradient of  $\text{MeOH}/\text{H}_2\text{O}$  (70:30  $\rightarrow$  75:25, v/v) to give **1** (3.5 mg). Fr. I5I was successively subjected to CC on silica gel eluting with a gradient of  $\text{CHCl}_3/\text{MeOH}$  (100:1  $\rightarrow$  80:1, v/v) and Sephadex HW-40F eluting with MeOH to yield **3** (15.5 mg).

Fr. H (12.5 g) was subjected to MCI gel column eluting with a gradient of  $\text{MeOH}/\text{H}_2\text{O}$  (65:35  $\rightarrow$  100:0, v/v) to afford eight fractions (Fr. H1–H8). Fr. H2, H3, and H4 were separated over ODS C-18 eluting with a gradient of  $\text{MeOH}/\text{H}_2\text{O}$  (65:35  $\rightarrow$  80:20, v/v) to furnish Fr. H2A–H2C, Fr. H3A–H3H, and Fr. H4A–H4K, respectively. Fr. H2B was further purified by silica gel CC eluting with a gradient of petroleum ether/acetone (5:1  $\rightarrow$  4:1, v/v) to afford **5** (6.1 mg). Fr. H3E and H4J were further separated by silica gel CC eluting with a gradient of petroleum ether/acetone (6:1  $\rightarrow$  3:1, v/v) to give **13** (7.1 mg) and **4** (5.9 mg), respectively. **8** (9.9 mg) was obtained from Fr. H4F by silica gel CC eluting with petroleum ether/acetone (6:1, v/v). **9** (10.1 mg) was obtained from Fr. H4G by recrystallization in  $\text{CHCl}_3$ , while **2** (6.1 mg) was obtained from the filtrated stock by silica gel CC eluting with petroleum ether/acetone (2:1, v/v).

#### 4.3.1. Euphominoid M (1)

Colorless crystals; mp 188–189 °C;  $[\alpha]_D^{25}$ : +18 (c 0.1, MeOH); IR (KBr)  $\nu_{\text{max}}$ : 3463, 2918, 2874, 1415, 1043  $\text{cm}^{-1}$ ; For  $^1\text{H}$  and  $^{13}\text{C}$  NMR spectroscopic data, see Table 1; HRESIMS  $m/z$  357.2034  $[\text{M} + \text{Na}]^+$  (calcd for  $\text{C}_{20}\text{H}_{30}\text{NaO}_4$ , 357.2036).

#### 4.3.2. Euphominoid N (2)

White amorphous powder;  $[\alpha]_D^{25}$ : +12 (c 0.1, MeOH); UV (MeOH)  $\lambda_{\text{max}}$  (log  $\epsilon$ ): 234 (3.60) nm; CD (MeOH)  $\lambda_{\text{max}}$  ( $\Delta\epsilon$ ) 231 (5.52) nm; IR (KBr)  $\nu_{\text{max}}$  3443, 2970, 2931, 1672, 1380, 1059  $\text{cm}^{-1}$ ;  $^1\text{H}$  and  $^{13}\text{C}$  NMR spectroscopic data, see Table 1; HRESIMS  $m/z$  319.2276  $[\text{M} + \text{H}]^+$  (calcd for  $\text{C}_{20}\text{H}_{31}\text{O}_3$ , 319.2268).

#### 4.3.3. Euphominoid O (3)

Pale-yellow oil;  $[\alpha]_D^{25}$ : –76 (c 0.1, MeOH); UV (MeOH)  $\lambda_{\text{max}}$  (log  $\epsilon$ ): 291 (3.51), 235 (3.16), 206 (3.20) nm; CD (MeOH)  $\lambda_{\text{max}}$  ( $\Delta\epsilon$ ) 237 (1.80), 289 (–5.53) nm; IR (KBr)  $\nu_{\text{max}}$ : 3418, 2920, 1959, 1652  $\text{cm}^{-1}$ ;  $^1\text{H}$  and  $^{13}\text{C}$  NMR spectroscopic data, see Table 1; HRESIMS  $m/z$  301.2176  $[\text{M} + \text{H}]^+$  (calcd for  $\text{C}_{20}\text{H}_{29}\text{O}_2$ , 301.2162).

#### 4.3.4. Euphominoid P (4)

Colorless crystals; mp 231–232 °C;  $[\alpha]_D^{25}$ : +70 (c 0.1, MeOH); IR (KBr)  $\nu_{\text{max}}$ : 3198, 2956, 2931, 2849, 1048, 1021  $\text{cm}^{-1}$ ;  $^1\text{H}$  and  $^{13}\text{C}$  NMR spectroscopic data, see Table 1; HRESIMS  $m/z$  327.2300  $[\text{M} + \text{Na}]^+$  (calcd for  $\text{C}_{20}\text{H}_{32}\text{NaO}_2$ , 327.2295).

#### 4.3.5. Euphominone C (5)

Colorless crystals; mp 185–186 °C;  $[\alpha]_D^{25}$ : –46 (c 0.1, MeOH); IR (KBr)  $\nu_{\text{max}}$ : 3496, 3397, 2969, 2922, 2857, 1680, 1378, 1042, 1002  $\text{cm}^{-1}$ ;  $^1\text{H}$  and  $^{13}\text{C}$  NMR spectroscopic data, see Table 2; HRESIMS  $m/z$  359.2207  $[\text{M} + \text{Na}]^+$  (calcd for  $\text{C}_{20}\text{H}_{32}\text{NaO}_4$ , 359.2193).

#### 4.3.6. Euphominone D (6)

Colorless crystals; mp 224–225 °C;  $[\alpha]_D^{25}$ : –6 (c 0.1, MeOH); IR (KBr)  $\nu_{\text{max}}$ : 3439, 3338, 2960, 2923, 2866, 1959, 1686, 1424, 1382, 1032  $\text{cm}^{-1}$ ;  $^1\text{H}$  and  $^{13}\text{C}$  NMR spectroscopic data, see Table 2; HRESIMS  $m/z$  343.2236  $[\text{M} + \text{Na}]^+$  (calcd for  $\text{C}_{20}\text{H}_{32}\text{NaO}_3$ , 343.2244).

#### 4.3.7. Euphominone E (7)

White amorphous powder;  $[\alpha]_D^{25}$ : +48 (c 0.1, MeOH); CD (MeOH)  $\lambda_{\text{max}}$

( $\Delta\epsilon$ ) 292 (12.8) nm; IR (KBr)  $\nu_{\text{max}}$ : 3466, 2927, 1682, 1379, 1040  $\text{cm}^{-1}$ ;  $^1\text{H}$  and  $^{13}\text{C}$  NMR spectroscopic data, see Table 2; HRESIMS  $m/z$  321.2432  $[\text{M} + \text{H}]^+$  (calcd for  $\text{C}_{20}\text{H}_{33}\text{O}_3$ , 321.2424).

#### 4.4. Crystallographic data of compounds 1, 4, 5, and 6

Single crystal of **1** was obtained from *n*-hexane/EtOAc (3:1, v/v) at 4 °C. Single crystals of **4**, **5**, and **6** were obtained from  $\text{CHCl}_3/\text{MeOH}/n$ -hexane/EtOAc (1:1:2:1, v/v),  $\text{CHCl}_3/\text{MeOH}/n$ -hexane/EtOAc (1:1:2:1, v/v), and  $\text{CHCl}_3$  at room temperature, respectively. The crystallographic data were obtained on a Bruker APEX II CCD diffractometer equipped with graphite-monochromatized  $\text{Cu K}\alpha$  radiation, and the structures were solved with the ShelXT (Sheldrick, 2015a) structure solution program using Intrinsic Phasing and refined with the ShelXL (Sheldrick, 2015b) refinement package using Least Squares minimization. The crystal was kept at 170.0 K during data collection using Olex2 (Dolomanov et al., 2009). The crystallographic data of **1**, **4**, **5**, and **6** were deposited in the Cambridge Crystallographic Data Centre. ORTEP drawings with a 30% ellipsoid probability level of the crystal structures of **1**, **4**, **5**, and **6** were depicted in Figs. 3 and 6–8, respectively.

##### 4.4.1. X-ray crystallographic data of 1

$\text{C}_{20}\text{H}_{30}\text{O}_4$ ,  $M = 334.44$  g/mol, monoclinic, space group C2,  $a = 28.9161(8)$  Å,  $b = 6.2294(2)$  Å,  $c = 23.6338(7)$  Å,  $\alpha = 90^\circ$ ,  $\beta = 124.1640(10)^\circ$ ,  $\gamma = 90^\circ$ ,  $V = 3522.51(19)$  Å<sup>3</sup>,  $Z = 8$ ,  $T = 170.0$  K,  $\mu(\text{Cu K}\alpha) = 0.689$   $\text{mm}^{-1}$ ,  $D_{\text{calc}} = 1.261$   $\text{g}/\text{cm}^3$ , 27163 reflections measured ( $4.518^\circ \leq 2\theta \leq 136.598^\circ$ ), 6451 unique ( $R_{\text{int}} = 0.0312$ ,  $R_{\text{sigma}} = 0.0224$ ), which were used in all calculations. The final  $R_1$  was 0.0353 ( $I > 2\sigma(I)$ ) and  $wR_2$  was 0.0950 (all data). The goodness of fit on  $F^2$  was 1.037. Flack parameter = 0.05(3).

##### 4.4.2. X-ray crystallographic data of 4

$\text{C}_{20}\text{H}_{32}\text{O}_2$ ,  $M = 304.45$  g/mol, orthorhombic, space group P2<sub>1</sub>2<sub>1</sub>2<sub>1</sub>,  $a = 7.7242(2)$  Å,  $b = 11.4575(4)$  Å,  $c = 20.1619(7)$  Å,  $\alpha = 90^\circ$ ,  $\beta = 90^\circ$ ,  $\gamma = 90^\circ$ ,  $V = 1784.33(10)$  Å<sup>3</sup>,  $Z = 4$ ,  $T = 170.0$  K,  $\mu(\text{Cu K}\alpha) = 0.544$   $\text{mm}^{-1}$ ,  $D_{\text{calc}} = 1.133$   $\text{g}/\text{cm}^3$ , 14226 reflections measured ( $8.772^\circ \leq 2\theta \leq 133.166^\circ$ ), 3131 unique ( $R_{\text{int}} = 0.0383$ ,  $R_{\text{sigma}} = 0.0294$ ), which were used in all calculations. The final  $R_1$  was 0.0294 ( $I > 2\sigma(I)$ ) and  $wR_2$  was 0.0724 (all data). The goodness of fit on  $F^2$  was 1.056. Flack parameter = 0.12(5).

##### 4.4.3. X-ray crystallographic data of 5

$\text{C}_{20}\text{H}_{32}\text{O}_4$ ,  $M = 336.45$  g/mol, monoclinic, space group P2<sub>1</sub>,  $a = 7.2021(9)$  Å,  $b = 10.5958(12)$  Å,  $c = 13.0458(16)$  Å,  $\alpha = 90^\circ$ ,  $\beta = 100.540(6)^\circ$ ,  $\gamma = 90^\circ$ ,  $V = 978.8(2)$  Å<sup>3</sup>,  $Z = 2$ ,  $T = 170.0$  K,  $\mu(\text{Cu K}\alpha) = 0.620$   $\text{mm}^{-1}$ ,  $D_{\text{calc}} = 1.142$   $\text{g}/\text{cm}^3$ , 12718 reflections measured ( $6.892^\circ \leq 2\theta \leq 137.48^\circ$ ), 3536 unique ( $R_{\text{int}} = 0.1088$ ,  $R_{\text{sigma}} = 0.0829$ ), which were used in all calculations. The final  $R_1$  was 0.0562 ( $I > 2\sigma(I)$ ) and  $wR_2$  was 0.1593 (all data). The goodness of fit on  $F^2$  was 1.041. Flack parameter = 0.00(17).

##### 4.4.4. X-ray crystallographic data of 6

$\text{C}_{20}\text{H}_{32}\text{O}_3$ ,  $M = 320.45$  g/mol, orthorhombic, space group P2<sub>1</sub>2<sub>1</sub>2<sub>1</sub>,  $a = 6.9340(3)$  Å,  $b = 11.1402(5)$  Å,  $c = 24.4859(10)$  Å,  $\alpha = 90^\circ$ ,  $\beta = 90^\circ$ ,  $\gamma = 90^\circ$ ,  $V = 1891.44(14)$  Å<sup>3</sup>,  $Z = 4$ ,  $T = 170.0$  K,  $\mu(\text{Cu K}\alpha) = 0.578$   $\text{mm}^{-1}$ ,  $D_{\text{calc}} = 1.125$   $\text{g}/\text{cm}^3$ , 55150 reflections measured ( $8.72^\circ \leq 2\theta \leq 136.85^\circ$ ), 3465 unique ( $R_{\text{int}} = 0.0308$ ,  $R_{\text{sigma}} = 0.0099$ ), which were used in all calculations. The final  $R_1$  was 0.0321 ( $I > 2\sigma(I)$ ) and  $wR_2$  was 0.0818 (all data). The goodness of fit on  $F^2$  was 1.064. Flack parameter = 0.05(2).

#### 4.5. ECD computational calculations

Conformational analyses were firstly carried out via Monte Carlo searching using molecular mechanism with MMFF force field in the Spartan 18 program (Wavefunction Inc.: Irvine, California, USA). Those

conformers were then re-optimized using DFT at the B3LYP/6-31G(d) level using the Gaussian 09 program (Frisch et al., 2009). The energies, oscillator strengths, and rotational strengths of the first 60 electronic excitations were calculated using the TDDFT methodology at the M062X/TZVP level in gas phase. The ECD spectra were simulated by the overlapping Gaussian function (Stephens et al., 2010). To get the conformationally averaged ECD spectra, the simulated spectra of the lowest energy conformers were averaged according to the Boltzmann distribution theory and their relative Gibbs free energy ( $\Delta G$ ).

#### 4.6. Bioassay

The  $\alpha$ -glucosidase inhibitory activity was evaluated using the methods we described previously (Ying et al., 2014, 2020), and the  $\beta$ -glucuronidase inhibitory assay was performed according to the method report (Zhou et al., 2020).

#### Declaration of competing interest

The authors declare that they have no known competing financial interests or personal relationships that could have appeared to influence the work reported in this paper.

#### Acknowledgments

The project was financially supported by the National Natural Science Foundation of China (No. 81872777).

#### Appendix A. Supplementary data

Supplementary data to this article can be found online at <https://doi.org/10.1016/j.phytochem.2022.113106>.

#### References

- Abad, A., Agulló, C., Cuñat, A.C., de Alfonso Marzal, I., Gris, A., Navarro, I., Ramírez de Arellano, C., 2007. Diastereoselective synthesis of antiqorin and related polyoxygenated atisene-type diterpenes. *Tetrahedron* 63, 1664–1679. <https://doi.org/10.1016/j.tet.2006.11.083>.
- Baraza, L.D., Joseph, C.C., Munissi, J.J., Nkonya, M.H., Arnold, N., Porzel, A., Wessjohann, L., 2008. Antifungal rosane diterpenes and other constituents of *Hugonia castaneifolia*. *Phytochemistry* 69, 200–205. <https://doi.org/10.1016/j.phytochem.2007.06.021>.
- Bhatt, A.P., Pellock, S.J., Biernat, K.A., Walton, W.G., Wallace, B.D., Creekmore, B.C., Letertre, M.M., Swann, J.R., Wilson, L.D., Roques, J.R., Darr, D.B., Bailey, S.T., Montgomery, S.A., Roach, J.M., Azcarate-Peril, M.A., Sartor, R.B., Gharaibeh, R.Z., Bultman, S.J., Redinbo, M.R., 2020. Targeted inhibition of gut bacterial  $\beta$ -glucuronidase activity enhances anticancer drug efficacy. *Proc. Natl. Acad. Sci. U.S.A.* 117, 7374–7381. <https://doi.org/10.1073/pnas.1918095117>.
- Cambie, R.C., Clark, G.R., Lal, A.R., Rickard, C.E.F., Rutledge, P.S., Woodgate, P.D., 1990. Structure and absolute configuration of two *ent*-atisane diterpenes from *Euphorbia fidjiana*. *Acta Crystallogr. C* 46, 2387–2389. <https://doi.org/10.1107/S0108270190003195>.
- Dolomanov, O.V., Bourhis, L.J., Gildea, R.J., Howard, J.A.K., Puschmann, H.J., 2009. OLEX2: a complete structure solution, refinement and analysis program. *Appl. Crystallogr.* 42, 339–341. <https://doi.org/10.1107/S0021889808042726>.
- Frisch, M.J., Trucks, G.W., Schlegel, H.B., Scuseria, G.E., Robb, M.A., Cheeseman, J.R., Scalmani, G., Barone, V., Mennucci, B., Petersson, G.A., Nakatsuji, H., Caricato, M., Li, X., Hratchian, H.P., Izmaylov, A.F., Bloino, J., Zheng, G., Sonnenberg, J.L., Hada, M., Ehara, M., Toyota, K., Fukuda, R., Hasegawa, J., Ishida, M., Nakajima, T., Honda, Y., Kitao, O., Nakai, H., Vreven, T., Montgomery Jr., J.A., Peralta, J.E., Ogliaro, F., Bearpark, M., Heyd, J.J., Brothers, E., Kudin, K.N., Staroverov, V.N., Kobayashi, R., Normand, J., Raghavachari, K., Rendell, A., Burant, J.C., Iyengar, S.S., Tomasi, J., Cossi, M., Rega, N., Millam, J.M., Klene, M., Knox, J.E., Cross, J.B., Bakken, V., Adamo, C., Jaramillo, J., Gomperts, R., Stratmann, R.E., Yazyev, O., Austin, A.J., Cammi, R., Pomelli, C., Ochterski, J.W., Martin, R.L., Morokuma, K., Zakrzewski, V.G., Voth, G.A., Salvador, P., Dannenberg, J.J., Dapprich, S., Daniels, A.D., Farkas, Ö., Foresman, J.B., Ortiz, J.V., Cioslowski, J., Fox, D.J., 2009. Gaussian 09, Revision A.1. Gaussian, Inc., Wallingford CT.
- Ghanadian, S.M., Ayatollahi, A.M., Mosaik, M.A., Abdalla, O.M., 2013. New immunosuppressive cyclomycinol diterpenes from *Euphorbia kopetdaghi* Prokh. *Nat. Prod. Res.* 27, 246–254. <https://doi.org/10.1080/14786419.2012.671318>.
- Gu, Q., Xu, J., Liu, S.N., 2017. Isolation of *Euphorbia Milii* Extracts Useful for the Treatment of EBV Virus Infection. *CN201611208207.3*.
- Hasan, A., Liu, G.Y., Hu, R., Aisa, H.A., 2019. Jatrophone diterpenoids from *Euphorbia glomerulans*. *J. Nat. Prod.* 82, 724–734. <https://doi.org/10.1021/acs.jnatprod.8b00507>.
- Hua, J., Luo, S.H., Liu, Y., Liu, Y.C., Tan, Y.Y., Feng, L., Xiao, C.J., Zhang, K.Q., Li, S.H., Niu, X.M., 2017. New bioactive macrocyclic diterpenoids from *Euphorbia helioscopia*. *Chem. Biodivers.* 14, e1700327. <https://doi.org/10.1002/cbdv.201700327>.
- Huang, Y.S., Lu, Y., Chen, C.H., Lee, K.H., Chen, D.F., 2019. Potent anti-HIV ingenane diterpenoids from *Euphorbia ebracteolata*. *J. Nat. Prod.* 82, 1587–1592. <https://doi.org/10.1021/acs.jnatprod.9b00088>.
- Keating, G.M., 2012. Ingenol mebutate gel 0.015% and 0.05%: in actinic keratosis. *Drugs* 72, 2397–2405. <https://doi.org/10.2165/11470090-000000000-00000>.
- Kemboi, D., Peter, X., Langat, M., Tembu, J., 2020. A Review of the ethnomedicinal uses, biological activities, and triterpenoids of *Euphorbia* species. *Molecules* 25, 4019–4048. <https://doi.org/10.3390/molecules25174019>.
- Kuang, X., Li, W., Kanno, Y., Yamashita, N., Nemoto, K., Asada, Y., Koike, K., 2016. *ent*-Atisane diterpenoids from *Euphorbia fischeriana* inhibit mammosphere formation in MCF-7 Cells. *J. Nat. Med.* 70, 120–126. <https://doi.org/10.1007/s11418-015-0940-6>.
- Kusz, N., Orvos, P., Csorba, A., Talosi, L., Chaieb, M., Hohmann, J., Redei, D., 2016. Jatrophone diterpenes from *Euphorbia guyoniana* are new potent inhibitors of atrial girk channels. *Tetrahedron* 72, 5724–5728. <https://doi.org/10.1016/j.tet.2016.08.007>.
- Kusz, N., Orvos, P., Bereczki, L., Fertey, P., Bombicz, P., Csorba, A., Talosi, L., Jakab, G., Hohmann, J., Redei, D., 2018. Diterpenoids from *Euphorbia dulcis* with potassium ion channel inhibitory activity with selective G protein-activated inwardly rectifying ion channel (GIRK) blocking effect. *J. Nat. Prod.* 81, 2483–2492. <https://doi.org/10.1021/acs.jnatprod.8b00500>.
- Lal, A.R., Cambie, R.C., Rutledge, P.S., Woodgate, P.D., 1990. *ent*-Atisane diterpenes from *Euphorbia fidjiana*. *Phytochemistry* 29, 1925–1935. [https://doi.org/10.1016/0031-9422\(90\)85042-E](https://doi.org/10.1016/0031-9422(90)85042-E).
- Liang, Y., An, L.J., Shi, Z.Y., Zhang, X.K., Xie, C.F., Tuerhong, M., Song, Z.H., Ohizumi, Y., Lee, D., Shuai, L., Xu, J., Guo, Y.Q., 2019. Bioactive diterpenoids from the stems of *Euphorbia antiqorum*. *J. Nat. Prod.* 82, 1634–1644. <https://doi.org/10.1021/acs.jnatprod.9b00134>.
- Liu, S.N., Huang, D., Morris-Natschke, S.L., Ma, H., Liu, Z.H., Seeram, N.P., Xu, J., Lee, K.H., Gu, Q., 2016. Euphomilones A and B, *ent*-rosane diterpenoids with 7/5/6 and 5/7/6 skeletons from *Euphorbia milii*. *Org. Lett.* 18, 6132–6135. <https://doi.org/10.1021/acs.orglett.6b03142>.
- Liu, S.N., Hu, J.Y., Tan, S.H., Wang, Q., Xu, J., Wang, Y., Yuan, Y., Gu, Q., 2017. *ent*-Rosane diterpenoids from *Euphorbia milii* showing an Epstein–Barr virus lytic replication assay. *RSC Adv.* 7, 46938–46947. <https://doi.org/10.1039/C7RA08877A>.
- Mai, Z.P., Ni, G., Liu, Y.F., Li, L., Li, J.Y., Yu, D.Q., 2018. Heliojatropones A and B, two jatrophone-derived diterpenoids with a 5/10 fused-ring skeleton from *Euphorbia helioscopia*: structural elucidation and biomimetic conversion. *Org. Lett.* 20, 3124–3127. <https://doi.org/10.1021/acs.orglett.8b01215>.
- Marston, A., Hecker, E., 1983. On the active principles of the *Euphorbiaceae*. VI: isolation and biological activities of seven milliamines from *Euphorbia milii*. *Planta Med.* 47, 141–147. <https://doi.org/10.1055/s-2007-969973>.
- Marston, A., Hecker, E., 1984. Active principles of the *Euphorbiaceae*. VII. Milliamines H and I, peptide esters of 20-deoxy-5-epsilon-hydroxyphorbol from *Euphorbia milii*. *Planta Med.* 50, 319–322. <https://doi.org/10.1055/s-2007-969720>.
- Min, Z.D., Mizuo, M., Toshiyuki, T., Munekazu, I., Xu, G.Y., Huang, Q., 1989. A diterpene from *Euphorbia antiqorum*. *Phytochemistry* 28, 553–555. [https://doi.org/10.1016/0031-9422\(89\)80049-4](https://doi.org/10.1016/0031-9422(89)80049-4).
- Rawal, M.K., Shokohinia, Y., Chianese, G., Zolfaghari, B., Appendino, G., TagliatalataScalfati, O., Prasad, R., Di Pietro, A., 2014. Jatrophanes from *Euphorbia squamosa* as potent inhibitors of candida albicans multidrug transporters. *J. Nat. Prod.* 77, 2700–2706. <https://doi.org/10.1021/np500756z>.
- Sheldrick, G.M., 2015a. SHELXT—Integrated space-group and crystal-structure determination. *Acta Crystallogr. A* 71, 3–8. <https://doi.org/10.1107/S2053273114026370>.
- Sheldrick, G.M., 2015b. Crystal structure refinement with SHELXL. *Acta Crystallogr. C* 71, 3–8. <https://doi.org/10.1107/S2053229614024218>.
- Shi, Q.W., Su, X.H., Kiyota, H., 2008. Chemical and pharmacological research of the plants in genus *Euphorbia*. *Chem. Rev.* 108, 4295–4327. <https://doi.org/10.1021/cr078350s>.
- Stephens, P.J., Harada, N., 2010. ECD cotton effect approximated by the Gaussian curve and other methods. *Chirality* 22, 229–233. <https://doi.org/10.1002/chir.20733>.
- Tian, Y., Guo, Q.L., Xu, W.D., Zhu, C.G., Yang, Y.C., Shi, J.G., 2014. A minor diterpenoid with a new 6/5/7/3 fused-ring skeleton from *Euphorbia micractina*. *Org. Lett.* 16, 3950–3953. <https://doi.org/10.1021/ol501760h>.
- Vasaa, A., Hohmann, J., 2014. *Euphorbia* diterpenes: isolation, structure, biological activity, and synthesis. *Chem. Rev.* 114. <https://doi.org/10.1021/cr400541j>, 8579–8612.
- Wallace, B.D., Wang, H., Lane, K.T., Scott, J.E., Orans, J., Koo, J.S., Venkatesh, M., Jobin, C., Yeh, L.A., Mani, S., Redinbo, M.R., 2010. Alleviating cancer drug toxicity by inhibiting a bacterial enzyme. *Science* 330, 831–835. <https://doi.org/10.1126/science.1191175>.
- Wallace, B.D., Roberts, A.B., Pollet, R.M., Ingle, J.D., Biernat, K.A., Pellock, S.J., Venkatesh, M.K., Guthrie, L., O'Neal, S.K., Robinson, S.J., Dollinger, M., Figueroa, E., McShane, S.R., Cohen, R.D., Jin, J., Frye, S.V., Zamboni, W.C., Peperanney, C., Mani, S., Kelly, L., Redinbo, M.R., 2015. Structure and inhibition of microbiome beta-glucuronidases essential to the alleviation of cancer drug toxicity. *Cell Chem. Biol.* 22, 1238–1249. <https://doi.org/10.1016/j.chembiol.2015.08.005>.

- Wan, L.S., Nian, Y., Ye, C.J., Shao, L.D., Peng, X.R., Geng, C.A., Zuo, Z.L., Li, X.N., Yang, J., Zhou, M., Qiu, M.H., 2016a. Three minor diterpenoids with three carbon skeletons from *Euphorbia peplus*. *Org. Lett.* 18, 2166–2169. <https://doi.org/10.1021/acs.orglett.6b00787>.
- Wan, L.S., Chu, R., Peng, X.R., Zhu, G.L., Yu, M.Y., Li, L., Zhou, L., Lu, S.Y., Dong, J.R., Zhang, Z.R., Li, Y., Qiu, M.H., 2016b. Pepluane and paraliene diterpenoids from *Euphorbia peplus* with potential anti-inflammatory activity. *J. Nat. Prod.* 79, 1628. <https://doi.org/10.1021/acs.jnatprod.6b00206>.
- Wang, B., Wei, Y.L., Zhao, X.Y., Tian, X.G., Ning, J., Zhang, B.J., Deng, S., Li, D.W., Ma, X.C., Wang, C., 2018. Unusual *ent*-atisane type diterpenoids with 2-Oxopropyl skeleton from the roots of *Euphorbia ebracteolata* and their antiviral activity against human rhinovirus 3 and enterovirus 71. *Bioorg. Chem.* 81, 234–240. <https://doi.org/10.1016/j.bioorg.2018.08.029>.
- Wang, L., Yang, J., Kong, L.M., Deng, J., Xiong, Z.J., Huang, J.P., Luo, J.Y., Yan, Y.J., Hu, Y.K., Li, X.N., Li, Y., Zhao, Y., Huang, S.X., 2017. Natural and semisynthetic tiglane diterpenoids with new carbon skeletons from *Euphorbia dracunculoides* as a wnt signaling pathway inhibitor. *Org. Lett.* 19, 3911–3914. <https://doi.org/10.1021/acs.orglett.7b01813>.
- Wei, Y.L., Yu, Z.L., Huo, X.K., Tian, X.G., Feng, L., Huang, S.S., Deng, S., Ma, X.C., Jia, J.M., Wang, C., 2018. Diterpenoids from the roots of *Euphorbia fischeriana* and their inhibitory effects on  $\alpha$ -glucosidase. *J. Asian Nat. Prod. Res.* 20, 1–8. <https://doi.org/10.1080/10286020.2017.1367923>.
- Xu, J., Kang, J., Cao, X.R., Sun, X.C., Yu, S.J., Zhang, X., Sun, H.W., Guo, Y.Q., 2015. Characterization of diterpenes from *Euphorbia prolifera* and their antifungal activities against phytopathogenic fungi. *J. Agric. Food Chem.* 63, 5902–5910. <https://doi.org/10.1021/acs.jafc.5b02021>.
- Xu, Y., Tang, P.Y., Zhu, M., Wang, Y.L., Sun, D.J., Li, H., Chen, L.X., 2021. Diterpenoids from the genus *Euphorbia*: structure and biological activity (2013–2019). *Phytochemistry* 19, 112846. <https://doi.org/10.1016/j.phytochem.2021.112846>.
- Yan, X.L., Sang, J., Chen, S.X., Li, W., Tang, G.H., Gan, L.S., Yin, S., 2019. Euphorkanlide A, a highly modified ingenane diterpenoid with a C24 appendage from *Euphorbia kansuensis*. *Org. Lett.* 21, 4128–4131. <https://doi.org/10.1021/acs.orglett.9b01315>.
- Yang, D.S., Zhang, Y.L., Peng, W.B., Wang, L.Y., Li, Z.L., Wang, X., Liu, K.C., Yang, Y.P., Li, H.L., Li, X.L., 2013. Jatrofolane-type diterpenes from *Euphorbia sikkimensis*. *J. Nat. Prod.* 76, 265–269. <https://doi.org/10.1021/np300799n>.
- Ying, Y.M., Zhang, L.Y., Zhang, X., Bai, H.B., Liang, D.E., Ma, L.F., Shan, W.G., Zhan, Z.J., 2014. Terpenoids with  $\alpha$ -glucosidase inhibitory activity from the submerged culture of *Inonotus obliquus*. *Phytochemistry* 108, 171–176. <https://doi.org/10.1016/j.phytochem.2014.09.022>.
- Ying, Y.M., Yu, H.F., Tong, C.P., Shan, W.G., Zhan, Z.J., 2020. Spiroinonotsuoxotriols A and B, two highly rearranged triterpenoids from *Inonotus obliquus*. *Org. Lett.* 22, 3377–3380. <https://doi.org/10.1021/acs.orglett.0c00866>.
- Yu, Z.L., Wei, Y.L., Tian, X.G., Yan, Q.L., Yan, Q.S., Huo, X.K., Wang, C., Sun, C.P., Zhang, B.J., Ma, X.C., 2018. Diterpenoids from the roots of *Euphorbia ebracteolata* and their anti-tuberculosis effects. *Bioorg. Chem.* 77, 471–477. <https://doi.org/10.1016/j.bioorg.2018.02.007>.
- Zani, C.L., Marston, A., Hamburger, M., Hostettmann, K., 1993. Molluscicidal milliamines from *Euphorbia milii* var. *hislopii*. *Phytochemistry* 34, 89–95. [https://doi.org/10.1016/S0031-9422\(00\)90788-X](https://doi.org/10.1016/S0031-9422(00)90788-X).
- Zhang, C.Y., Wu, Y.L., Zhang, P., Chen, Z.Z., Li, H., Chen, L.X., 2019. Anti-inflammatory lathyrene diterpenoids from *Euphorbia lathyris*. *J. Nat. Prod.* 82, 756–764. <https://doi.org/10.1021/acs.jnatprod.8b00600>.
- Zhao, J.X., Liu, C.P., Qi, W.Y., Han, M.L., Han, Y.S., Wainberg, M.A., Yue, J.M., 2014. Eurifoloids A–R, structurally diverse diterpenoids from *Euphorbia nerifolia*. *J. Nat. Prod.* 77, 2224–2233. <https://doi.org/10.1021/np5004752>.
- Zhou, B., Wu, Y., Dalal, S., Cassera, M.B., Yue, J.M., 2016. Euphorbesulins A–P, structurally diverse diterpenoids from *Euphorbia esula*. *J. Nat. Prod.* 79, 1952–1961. <https://doi.org/10.1021/acs.jnatprod.6b00205>.
- Zhou, T.S., Wei, B., He, M., Li, Y.S., Wang, Y.K., Wang, S.J., Chen, J.W., Zhang, H.W., Cui, Z.N., Wang, H., 2020. Thiazolidin-2-cyanamides derivatives as novel potent *Escherichia coli*  $\beta$ -glucuronidase inhibitors and their structure-inhibitory activity relationships. *J. Enzym. Inhib. Med. Chem.* 35, 1736–1742. <https://doi.org/10.1080/14756366.2020.1816998>.